International Journal of Mechanical Sciences 161–162 (2019) 105024

Contents lists available at ScienceDirect

International Journal of Mechanical Sciences

journal homepage: www.elsevier.com/locate/ijmecsci

An analytical solution for elastic buckling analysis of stiffened panel subjected to pure bending

Wenbin Zhou, Yong Li, Zhusheng Shi*, Jianguo Lin

Department of Mechanical Engineering, Imperial College London, London SW7 2AZ, UK

ARTICLE INFO

Keywords:
Buckling analysis
Stiffened panel
Analytical solution
Bending
Effective width

ABSTRACT

In this study, an analytical solution has been developed for the elastic buckling analysis of stiffened panels subjected to pure bending, and the effect of main geometric parameters of the stiffened panels on buckling strength has been investigated. A simplified model of stiffened panels has been proposed for buckling analysis, where an elastically built-in boundary condition replaces the skin's effect on buckling of the stiffened panels. The equilibrium method with a conventional rigid skin assumption and a new flexible skin assumption is developed for the simplified model to analytically capture the buckling behaviour of the stiffened panels. To consider the non-rigid rotation effect of flexible skin on buckling of stiffened panels, a new parameter, the effective width of stiffened panels, has been introduced, and a finite element (FE) assisted method has been employed to obtain its value for different stiffened panels. The results show that the flexible skin assumption significantly enhances the accuracy of buckling strength prediction compared with the conventional rigid skin assumption, and the maximum difference between analytical results and corresponding FE simulations is decreased from 12.2% with rigid skin assumption to only 3.9%. Based on the proposed analytical solution, effects of main geometric parameters of the stiffened panels (the stiffened panel length and width, the stiffener height, and the ratio of the skin thickness to the stiffener thickness) on their buckling coefficients have been discussed. Increasing stiffened panel length and/or reciprocal of stiffener height leads to an initial abrupt decrease of the buckling coefficient until reaching a stable level. When the stiffened panel width increases, the buckling coefficient first increases and then remains stable, whereas increasing thickness ratio leads to the increase of the buckling coefficient.

1. Introduction

Stiffened panels are widely used in marine and aerospace applications due to their lightweight and high bending stiffness characteristics [1]. Different methods have been employed to produce stiffened panels [2]. The conventional built-up stiffened panels are manufactured by connecting the formed skins and stiffeners through welding [3] or riveting technologies [4]. The integrally stiffened panels, which are machined or extruded from a single thick plate [1], become more and more popular, due to their advantages of higher crack growth life and lower manufacturing cost compared with built-up stiffened panels [5]. Some forming technologies, such as press bend forming [6,7] and creep age forming [5,8], have been reported to be suitable methods for forming integrally stiffened panels into desired shapes. More recently, Hua and co-workers developed a new Space Envelope Forming (SEF) method, in which the envelope of motion paths of a rocking tool on workpiece forms the profile of components, for manufacturing integral thin-walled high web rib panels [9]. They have also developed theories for calculating the rocking die motion track to design non-rotary rocking tool and for interference judgement between the rocking tool and components, and have applied non-rotary rocking tools to produce thin-walled gear (under circular motion) [10,11] and thin-walled gear rack (under straight motion) [12]. These pioneer experimental [10] and theoretical [11] achievements have opened a new scope for the manufacturing of lightweight panels with integrated stiffeners.

Flat stiffened panels are often formed to desired shapes for particular applications by different forming technologies such as creep age forming, during which bending is one of the most common loading conditions. Buckling may occur in the stiffener area of the stiffened panels during bending due to the high concentrated stresses at the top of the stiffeners, which could lead to failure of stiffened panels in the forming process [13]. On the other hand, stiffener design can be optimised to avoid possible buckling problem. Hence, in order to achieve the successful forming and guide the design of stiffened panels, it is necessary to understand their buckling behaviour subjected to bending conditions.

* Corresponding author.
E-mail address: zhusheng.shi@imperial.ac.uk (Z. Shi).

https://doi.org/10.1016/j.ijmecsci.2019.105024
Received 12 May 2019; Received in revised form 25 June 2019; Accepted 15 July 2019
Available online 15 July 2019

Nomenclature

a	Length of stiffened panel (mm)
A	Area (mm^2)
A_{ij}	Coefficient of linear homogeneous equations (–)
b	Width of stiffened panel (mm)
b_{eff}	Effective width of stiffened panel (mm)
$C_{m,n}$	Coefficient of deflection function of stiffened panel (–)
C_r	Non-dimensional rotational constraint coefficient of skin (–)
D	Flexural stiffness of stiffener (GPa mm^3)
E	Young's modulus (GPa)
f_m	Deflection function of stiffened panel in the y-direction with respect to numbers of half-waves (–)
f_m'', $f_m^{(4)}$	The second and fourth derivatives of f_m (–)
G	Shear modulus (GPa)
h	Height of stiffener (mm)
J_{sk}, J'_{sk}	Polar moment of inertia of rigid skin and flexible skin respectively (mm^4)
k, k_{cr}	Non-dimensional buckling coefficient and its critical value (–)
$[k]$, $[k]_G$	Stiffness matrices and geometric stiffness matrices respectively (–)
m	Number of half-waves in the x-direction in a buckling mode (–)
M_c	Moment per unit length applied on connecting edge of stiffener by skin which acts as a bending moment ((N m)/m)
M'_c	Moment per unit length applied on connecting edge of skin by stiffener which acts as a torsional moment ((N m)/m)
M'_{c0}	Moment per unit length at joint of connecting edge and symmetric line ((N m)/m)
M_{cr}	Critical buckling moment (N m)
M_{up}	Moment per unit length on upper edge of stiffened panel ((N m)/m)
M_z	Moment applied on stiffened panel in the z-direction (N m)
n	Non-negative integer (–)
t_{sk}, t_{st}	Thickness of skin and stiffener respectively (mm)
V_{up}	Vertical shearing force per unit length along upper edge of stiffened panel (N/m)
w	Deflection of stiffener in the z-direction (mm)
x, y, z	Coordinates (–)
Δx	Spatial increment of neighbouring nodes (mm)
y_0	Distance between neutral axis of stiffened panel and top of stiffened panel (mm)
α	Loading coefficient (–)
$\{\delta\}$	Buckling eigenvector (–)
ξ, η	Non-dimensional coordinates in x and y-directions, defined as x/a and y/b respectively (–)
θ, θ'	Rotation angle of skin and stiffener respectively (rad)
θ_f, θ_r	Rotation angle of flexible skin and rigid skin respectively (rad)
λ	Buckling load eigenvalue (–)
μ	Deflection of skin in the y-direction (mm)
ν	Poisson's ratio (–)
σ_x	In-plane stress in the x-direction (MPa)
σ_{cr}	Critical buckling strength (MPa)
σ_0	In-plane stress in the x-direction at top of stiffener (MPa)

Finite element (FE) method has been used to calculate critical buckling strengths of stiffened panels under different loading conditions, such as compression and bending, whose effectiveness has been validated by some buckling tests [14,15]. However, a long simulation time is needed to obtain accurate results. The total simulation time could be significantly long in the design of stiffened panels, as an iterative optimisation is generally needed and the critical buckling strength has to be calculated at each iteration [16]. Hence, analytical solutions for buckling analysis of stiffened panels, which can achieve comparatively accurate results in an extremely short time, is very much in need [17].

Currently, two main analytical methods are generally used to solve the buckling behaviour of structures: the equilibrium method and the energy method (Ritz method). In the equilibrium method, the equilibrium differential equation of buckling is directly solved based on the loading and deflection functions of the structures with corresponding boundary constraint equations [18,19]. The equilibrium method can obtain exact results of critical buckling strength with high efficiency and has been widely employed for buckling strength calculations of thin plates with different loading and boundary conditions, such as simply supported thin plates under uniform compression [20,21] or under linearly distributed stress [22,23]. The method has also been successfully applied to the buckling analysis of stiffened panels under loading conditions where buckling mainly occurs on the skin, such as compression [24] and eccentric compression along skin [25]. In these cases, the equilibrium equations in the skin of the stiffened panels were used for the buckling calculations and the effect from the stiffener on buckling was considered by adding a special constraint, elastically built-in (an intermediate boundary condition between simply supported and built-in condition), on the joint edge between the skin and stiffener [26]. For example, Paik and Thayambali [27] analysed the skin buckling behaviour of stiffened panels with multi-stiffener, where the section of the skin between two stiffeners was modelled as a thin plate with two elastically built-in boundaries. Under many other loading conditions, such as bending, buckling of stiffened panels also occurs in the stiffener. However, no report has been found to solve the buckling problem in the stiffener of the stiffened panels using the equilibrium method.

The energy method, on the other hand, solves the buckling problems in terms of the total potential energy which is the sum of the strain energy stored in the structure (depending on the deflection of structure) and the work done of the applied load (relating to critical buckling strength). The buckling stress is obtained by minimising the total potential energy [28]. The method is much easier to be applied to buckling calculations for structures with complicated geometric conditions, such as stiffened panels, however, the deflection of the buckled structures has to be assumed before the calculations, which raises some uncertainties of the method [29]. Energy method has been applied to calculate the buckling strength of stiffened panels in many studies [30], however, different flexible skin deflection assumptions have been used to consider the interaction between skin and stiffener, such as one half-waves or two half-waves deflection assumptions [31,32] and deflections defined by trigonometric functions [33,34]. The main limitation of the energy method is that the deflections of the buckled structures are assumed empirically, which is hard to guarantee the accuracy of the calculated results.

In this paper, a buckling analysis based on the equilibrium method is developed for stiffened panels subjected to bending in the elastic region, which is simplified as a stiffener with rotational constraints from the skin. The equilibrium equation of buckling in the equilibrium method is solved by the Frobenius method to acquire the critical buckling strength of stiffened panels under a bending moment. A new parameter, the effective width of stiffened panel, is introduced into the buckling analysis to consider the effect of non-rigid rotation of the flexible skin. FE simulations of some selected cases have been carried out to compare with the corresponding analytical results and verify the accuracy of the proposed analytical solution. Furthermore, the effects of the main geometric parameters of stiffened panels on the critical buckling strength have been investigated and discussed based on both the analytical and numerical results.

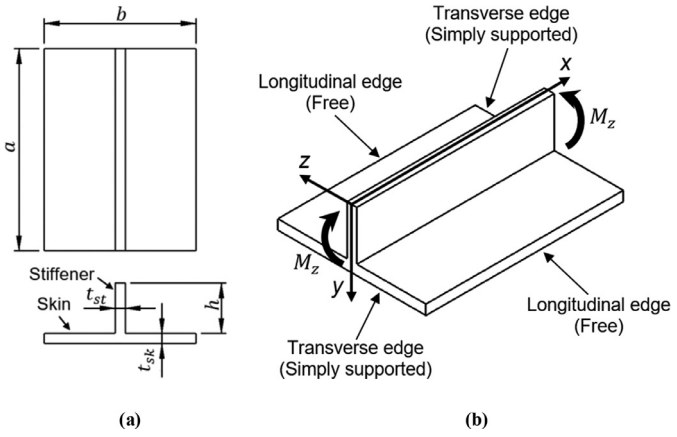

Fig. 1. Schematic diagram of a single blade stiffened panel subjected to bending: (a) the geometric parameters and (b) the boundary conditions.

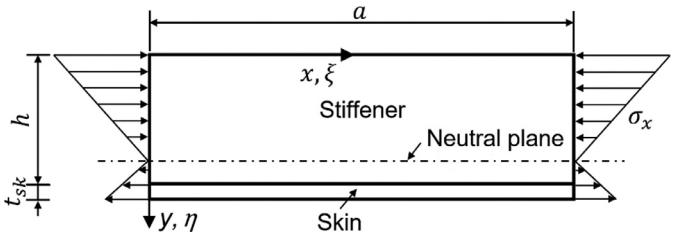

Fig. 2. Schematic showing the x-directional stress distribution (σ_x) along the y-axis of a stiffened panel subjected to bending.

2. Problem definition

2.1. Stiffened panels subjected to pure bending

The buckling behaviour of stiffened panels with a single high blade stiffener subjected to a bending moment is studied in this paper. Fig. 1 shows the geometric parameters and boundary conditions of the stiffened panel subjected to pure bending, in which a coordinate system has been defined. The main geometric parameters that affect the buckling behaviour of the stiffened panels include the stiffened panel length a, the stiffened panel width b, the skin thickness t_{sk}, the stiffener height h and the stiffener thickness t_{st}, as shown in Fig. 1(a). The bending moment M_z is applied on the two transverse edges of the stiffened panel ($x=0,\ x=a$) during the loading process. The boundary conditions of the bending stiffened panel are demonstrated in Fig. 1(b). Two transverse edges of the stiffened panel are defined as simply supported, while the two longitudinal edges are treated as free. Since the thicknesses of the stiffened panels are relatively small compared with other dimensions (width and length), both the stiffener and the skin of the stiffened panels can be represented as thin plates. Therefore, these two structures are assumed to follow the Kirchhoff–Love plate theory in this study.

2.2. Stress distributions

According to the Kirchhoff–Love plate theory, a linearly varying stress is distributed along the y-direction of stiffened panels loaded by the bending moment M_z. Fig. 2 illustrates a sketch of the stress distribution in the bending stiffened panel. The in-plane stress of the stiffened panel in the x-direction σ_x can be expressed as:

$$\sigma_x = -\sigma_0\left(1-\alpha\frac{y}{h}\right) = -\sigma_0(1-\alpha\eta)\ \left(0\le\eta\le\left(h+t_{sk}\right)/h\right) \tag{1}$$

where $\eta=y/h$ is a normalised y-coordinate and the normalised x-coordinates is also defined, as $\xi=x/a$. σ_0 is the x-directional stress at the top of the stiffener ($\eta=0$), indicating the maximum compressive stress in the bent stiffened panel. α is a loading coefficient which describes the stress distribution and is determined by the stiffener height and the distance between the neutral plane and the top of the stiffened panel y_0:

$$\alpha = \frac{h}{y_0} \tag{2}$$

where

$$y_0 = \frac{\int y\,dA}{\int dA} = \frac{t_{st}\frac{h^2}{2}+t_{sk}b\left(h+\frac{t_{sk}}{2}\right)}{t_{st}h+t_{sk}b} \tag{3}$$

When the stiffened panel is subjected to a bending moment, the loading coefficient α ranges from 1 to 2.

Divide both numerator and denominator in Eq. (3) by h, Eq. (3) becomes:

$$y_0 = \frac{\frac{h}{2}+b\frac{t_{sk}}{t_{st}}\left(1+\frac{t_{sk}}{2h}\right)}{1+\frac{t_{sk}}{t_{st}}\frac{b}{h}} \tag{4}$$

Since high stiffener conditions are considered in this study, the skin thickness is much smaller than the stiffener height and then the item $t_{sk}/2h \ll 1$ in Eq. (4). Therefore, there are three main parameters that affect y_0 according to Eq. (4), including the stiffener height h, the stiffened panel width b and the thickness ratio t_{sk}/t_{st}.

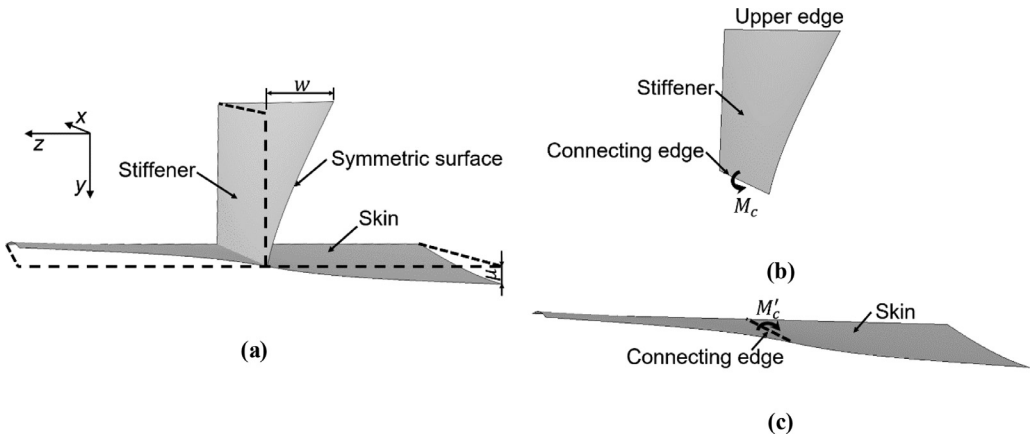

Fig. 3. Buckling mode of stiffened panels subjected to pure bending: (a) stiffener buckling mode, and breakdown diagrams of the free body of (b) the stiffener and (c) the skin.

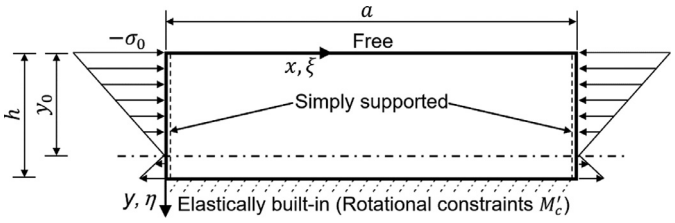

Fig. 4. Simplified model for buckling analysis of stiffened panels loaded by bending moment.

2.3. Buckling mode and buckling model

There are three types of buckling modes for stiffened panels when subjected to different loading conditions, including Euler buckling (overall buckling), skin buckling and stiffener buckling. For the case of stiffened panels loaded by pure bending investigated in this study (Fig. 1(b)), the top of the stiffener is in compression and the skin is in tension, therefore, buckling would firstly occur in the stiffener section and the primary buckling mode should be the stiffener buckling. Fig. 3(a) demonstrates the general stiffener buckling mode, in which w is the deflection of the stiffener in the z-direction, representing the occurrence of buckling, and μ is the deflection of the skin in the y-direction due to the torsion applied by the stiffener.

In order to facilitate the analytical solution of the complicated buckling problem of stiffened panels, the stiffener and the skin sections of the stiffened panel can be analysed individually, as illustrated in Fig. 3(b) and (c). The stiffener section is subjected to a distribution of linearly varying stress of σ_x at the two transverse edges of $x=0$ and $x=a$ (Fig. 2) and the constraints from the skin can be replaced by a bending moment M_c at the connecting edge, as shown in Fig. 3(b). The skin section is loaded by tension at two transverse edges (Fig. 2) and a moment M_c' along the connecting edge acts as a torsion moment to the skin due to the buckling of the stiffener. The bending moment M_c is the reaction of the torsional moment M_c' and their magnitude is equal. As the stiffener section is the primary buckling area in the stiffened panels under bending investigated in this study, the buckling problem can be simplified to consider the stiffener section only. The effect from the skin section (the rotational constraint M_c' in Fig. 3(b)) can be represented by an elastically built-in constraint in the connecting edge, as shown in Fig. 4 [16].

The simplified model of buckling of stiffened panels subjected to pure bending then can be considered as a thin stiffener with two simply supported loading edges ($x=0$, $x=a$), one restrained connecting edge ($y=h$) and one free edge ($y=0$), as shown in Fig. 4. The connecting edge is equivalently constrained by an elastically built-in boundary condition which restricts the movement in the z-direction and the rotation in the yz-plane of the connecting edge by a torsional moment M_c'.

The skin rotational constraint of the elastically built-in boundary condition is determined by $M_c + M_c' = 0$ along the connecting edge, as illustrated in Fig. 3. Based on Saint Venant's torsion theory [35], M_c' can be calculated analytically following the rigid skin assumption, where the cross section of skin in the yz-plane remains straight after deformation, as shown in Fig. 5(a), in which θ is the rotation angle of the rigid skin and θ' is the rotation angle of the stiffener baseline after buckling. The rigid skin assumption is a correct approximation if the skin does not distort [16]. However, in practical situations, the skin generally rotates flexibly with distortions, as shown in Fig. 5(b). The analytical solutions considering the practical flexible skin case cannot be performed directly since the deformation of flexible skin under torsion is too complicated to be analytically modelled [36]. Hence, a compensation method for the flexible skin case with the assistance from FE simulations has been proposed in this study and will be introduced later.

2.4. Boundary conditions of buckling model

M_c' is determined by the rotation angle of the skin θ and the torsional stiffness of the skin based on the rigid skin assumption, while M_c is determined by the deflection of the stiffener w and the flexural stiffness of the stiffener D. According to the rotational continuity condition along the skin-stiffener intersection [33], the rotation angle of the skin θ is equal to the rotation angle of the stiffener baseline θ', which gives:

$$\theta = \theta' = \left(\frac{\partial w}{\partial y}\right)_{y=h} \tag{5}$$

Base on Eq. (5), M_c' can be expressed by the deflection of stiffener w:

$$M_c'|_{y=h} = \left(GJ_{sk}\frac{\partial}{\partial x}\frac{\partial^2 w}{\partial x \partial y}\right)_{y=h} \tag{6}$$

where GJ_{sk} is the torsional stiffness of the skin, in which G is the shear modulus of the material and J_{sk} is the polar moment of inertia of the skin in rigid skin assumption. G and J_{sk} can be expressed as:

$$G = \frac{E}{2(1+\upsilon)} \tag{7}$$

$$J_{sk} = \frac{bt_{sk}^3}{3} \tag{8}$$

where E and υ are respectively Young's modulus and Poisson's ratio of the material. In the simplified model, the upper edge is free and the connecting edge is elastically built-in. The boundary conditions of the simplified buckling model of stiffened panels can be represented mathematically as below:

(1) Free at the upper edge ($y=0$)

- The vertical shearing force V_{up} along the upper edge is free [20], which gives:

$$V_{up}|_{y=0} = D\left(\frac{\partial^3 w}{\partial y^3} + (2-\upsilon)\frac{\partial^3 w}{\partial x^2 \partial y}\right)_{y=0} = 0 \tag{9}$$

- The moment M_{up} along the upper edge is free [20], which gives:

$$M_{up}|_{y=0} = D\left(\frac{\partial^2 w}{\partial y^2} + \upsilon\frac{\partial^2 w}{\partial x^2}\right)_{y=0} = 0 \tag{10}$$

where D is the flexural stiffness of the stiffener, as:

$$D = \frac{Et_{st}^3}{12\left(1-\upsilon^2\right)} \tag{11}$$

(1) Elastically built-in at the connecting edge ($y=h$)

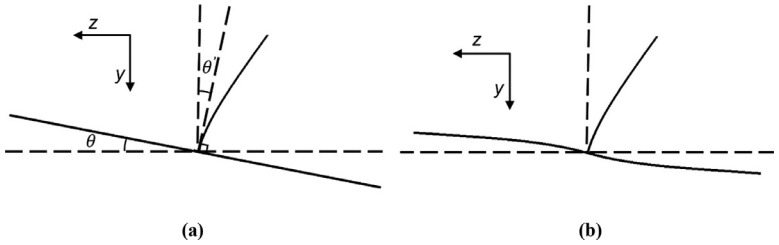

Fig. 5. Buckling of stiffened panels with (a) rigid skin and (b) flexible skin conditions.

- The deflection w along the connecting edge is zero:

$$w|_{y=h} = 0 \tag{12}$$

- The moment along the connecting edge is in an equilibrium condition:

$$M_c|_{y=h} + M_c'|_{y=h} = \left(D\left(\frac{\partial^2 w}{\partial y^2} + \upsilon \frac{\partial^2 w}{\partial x^2} \right) + GJ_{sk} \frac{\partial}{\partial x} \frac{\partial^2 w}{\partial x \partial y} \right)_{y=h} = 0 \tag{13}$$

Replacing x and y by corresponding normalised coordinates ξ and η, the boundary conditions in Eqs. (9), (10), (12) and (13) can be summarised as:

$$\begin{cases} \left(\frac{1}{h^3} \frac{\partial^3 w}{\partial \eta^3} + (2-\upsilon) \frac{1}{a^2 h} \frac{\partial^3 w}{\partial \xi^2 \partial \eta} \right)_{\eta=0} = 0 \\ \left(\frac{1}{h^2} \frac{\partial^2 w}{\partial \eta^2} + \upsilon \frac{1}{a^2} \frac{\partial^2 w}{\partial \xi^2} \right)_{\eta=0} = 0 \\ (w)_{\eta=1} = 0 \\ \left(D\left(\frac{1}{h^2} \frac{\partial^2 w}{\partial \eta^2} + \upsilon \frac{1}{a^2} \frac{\partial^2 w}{\partial \xi^2} \right) + GJ_{sk} \frac{1}{a^2 h} \frac{\partial}{\partial \xi} \frac{\partial^2 w}{\partial \xi \partial \eta} \right)_{\eta=1} = 0 \end{cases} \tag{14}$$

3. Analytical method

3.1. Buckling analysis with rigid skin case

In this section, the equilibrium method is used to solve the buckling problem of stiffened panels with the rigid skin case by the proposed simplified model. The partial differential form of the equilibrium equation for the model under a pure bending moment is given by [20]:

$$\frac{\partial^4 w}{\partial x^4} + 2 \frac{\partial^4 w}{\partial x^2 y^2} + \frac{\partial^4 w}{\partial y^4} = \frac{\sigma_x t_{st}}{D} \frac{\partial^2 w}{\partial x^2} \tag{15}$$

Using the normalised coordinates, the partial differential equation becomes:

$$\frac{h^4}{a^4} \frac{\partial^4 w}{\partial \xi^4} + 2 \frac{h^2}{a^2} \frac{\partial^4 w}{\partial \xi^2 \eta^2} + \frac{\partial^4 w}{\partial \eta^4} = \frac{h^2}{a^2} \frac{\sigma_x t_{st} h^2}{D} \frac{\partial^2 w}{\partial \xi^2} \tag{16}$$

For thin plates with the simply supported boundary condition, the free edges of the buckled plates have been reported to generally show sinusoidal half-waves patterns [28], and hence the deflection w in the free edge of stiffener along the x-direction can be modelled by the following equation [20]:

$$w = f_m(\eta) \sin(m\pi\xi) \tag{17}$$

where m is the number of sinusoidal half-waves in the x-direction, $f_m(\eta)$ is a function of η and m to describe the displacement in the z-direction, which satisfies the boundary conditions of the upper edge and the connecting edge of the simplified model.

Substituting σ_x in Eq. (1) and deflection w in Eq. (17) into Eq. (16), it becomes an ordinary differential equation:

$$\left(\frac{d^4 f_m}{d\eta^4} - 2\psi^2 \frac{d^2 f_m}{d\eta^2} + \psi^4 f_m \right) = \psi^2 \pi^2 \frac{\sigma_0 t_{st} h^2}{\pi^2 D} (1 - \alpha\eta) f_m \tag{18}$$

where $\psi = m\pi h/a$. To simplify Eq. (18), the buckling coefficient k, which is the non-dimensional form of buckling strength [20], is used and Eq. (18) becomes:

$$\frac{d^4 f_m}{d\eta^4} - 2\psi^2 \frac{d^2 f_m}{d\eta^2} + \left(\psi^4 - \psi^2 \pi^2 k (1 - \alpha\eta) \right) f_m = 0 \tag{19}$$

where

$$k = \frac{\sigma_0 t_{st} h^2}{\pi^2 D} \tag{20}$$

Since the differential equation Eq. (19) is a transcendental equation, it cannot be solved in a closed-form solution. Frobenius method is used to solve the differential equation by expressing $f_m(\eta)$ in a power series solution, as [22,23]:

$$f_m(\eta) = \sum_{n=0}^{\infty} C_{m,n} \eta^n \tag{21}$$

where $C_{m,n}$ is a coefficient related to the number of half-waves m and the number of power series n. The second and fourth derivatives of $f_m(\eta)$ in Eq. (19) can be expressed as:

$$\begin{aligned} f''_m(\eta) &= \sum_{n=0}^{\infty} (n+2)!/n! C_{m,n+2} \eta^n \\ f_m^{(4)}(\eta) &= \sum_{n=0}^{\infty} (n+4)!/n! C_{m,n+4} \eta^n \end{aligned} \tag{22}$$

Eq. (19) then can be updated as follows:

$$\sum_{n=1}^{\infty} \left\{ \left[\frac{(n+4)!}{n!} C_{m,n+4} - 2\psi^2 \frac{(n+2)!}{n!} C_{m,n+2} + \psi^2 \left(\psi^2 - \pi^2 k \right) C_{m,n} - \alpha\psi^2 \pi^2 k C_{m,n-1} \right] \eta^n \right\} + \left[24 C_{m,4} - 4\psi^2 C_{m,2} + \psi^2 \left(\psi^2 - \pi^2 k \right) C_{m,0} \right] \eta^0 = 0 \tag{23}$$

As Eq. (23) is satisfied for all η values, ranging from 0 to 1, the coefficients of η^0 and η^n ($n = 1, 2, 3, \ldots$) in Eq. (23) have to be zero, one obtains:

$$24 C_{m,4} - 4\psi^2 C_{m,2} + \psi^2 \left(\psi^2 - \pi^2 k \right) C_{m,0} = 0 \tag{24}$$

$$(n+4)!/n! C_{m,n+4} - 2\psi^2 (n+2)!/n! C_{m,n+2} + \psi^2 \left(\psi^2 - \pi^2 k \right) C_{m,n} - \alpha\psi^2 \pi^2 k C_{m,n-1} = 0 \ (n \geq 1) \tag{25}$$

$C_{m,4}$ then can be expressed by $C_{m,2}$, $C_{m,0}$ and the buckling coefficient k according to Eq. (24):

$$C_{m,4} = \frac{\psi^2}{24} \left(4 C_{m,2} - \left(\psi^2 - \pi^2 k \right) C_{m,0} \right) \tag{26}$$

The recursive equation of $C_{m,n+4}$ ($n = 1, 2, 3, \ldots$) can be given from Eq. (25):

$$C_{m,n+4} = \frac{n! \psi^2 \left(2(n+1)(n+2) C_{m,n+2} - \left(\psi^2 - \pi^2 k \right) C_{m,n} - \alpha\pi^2 k C_{m,n-1} \right)}{(n+4)!} \tag{27}$$

Therefore, $C_{m,n}$ ($n \geq 4$) can be expressed in terms of the first four coefficients $C_{m,0}$, $C_{m,1}$, $C_{m,2}$, $C_{m,3}$ and k according to Eqs. (26) and (27). The deflection of the stiffener w represented with four coefficients $C_{m,0}$, $C_{m,1}$, $C_{m,2}$, $C_{m,3}$ and k is then obtained by substituting Eqs. (21), (26) and (27) into Eq. (17).

The boundary condition is used to determine the buckling coefficient k. The boundary condition of the stiffened panel in Eq. (14) can be simplified by substituting Eq. (17), as:

$$\begin{cases} \left(\frac{\partial^3 f_m}{\partial \eta^3} + (2-\upsilon) \psi^2 \frac{\partial f_m}{\partial \eta} \right)_{\eta=0} = 0 \\ \left(\frac{\partial^2 f_m}{\partial \eta^2} + \upsilon \psi^2 \right)_{\eta=0} = 0 \\ (f_m)_{\eta=1} = 0 \\ \left(\frac{\partial^2 f_m}{\partial \eta^2} + C_r \frac{\partial f_m}{\partial \eta} \right)_{\eta=1} = 0 \end{cases} \tag{28}$$

where

$$C_r = \frac{GJ_{sk}}{D} \frac{m^2 \pi^2 h}{a^2} = 2m^2 \pi^2 (1-\upsilon) \frac{bh}{a^2} \frac{t_{sk}^3}{t_{st}^3} \tag{29}$$

C_r is the rotational constraint coefficient of the skin which is related to the width and length of the stiffened panel, the stiffener height and

the thickness ratio. C_r varies from 0 (free rotation) to ∞ (fixed rotation) in the elastically built-in condition [27]. Substitute Eq. (21) into the boundary condition of Eq. (28), the four boundary functions can be expressed by $C_{m,n}$:

$$\begin{cases} 2C_{m,2} + v\psi^2 C_{m,0} = 0 \\ 6C_{m,3} + (2-v)\psi^2 C_{m,1} = 0 \\ \sum_{n=1}^{\infty} C_{m,n} = 0 \\ \sum_{n=1}^{\infty} n(n-1)C_{m,n} + C_r \sum_{n=1}^{\infty} nC_{m,n} = 0 \end{cases} \tag{30}$$

Eq. (30) can be represented by a set of linear homogeneous equations using $C_{m,0}$, $C_{m,1}$, $C_{m,2}$, $C_{m,3}$, as:

$$\begin{bmatrix} A_{11} & A_{12} & A_{13} & A_{14} \\ A_{21} & A_{22} & A_{23} & A_{24} \\ A_{31} & A_{32} & A_{33} & A_{34} \\ A_{41} & A_{42} & A_{43} & A_{44} \end{bmatrix} \begin{Bmatrix} C_{m,0} \\ C_{m,1} \\ C_{m,2} \\ C_{m,3} \end{Bmatrix} = 0 \tag{31}$$

where A_{ij} ($i = 1 \sim 4$, $j = 1 \sim 4$) are the coefficients of the linear homogeneous equations, in which $A_{11} = v\psi^2$, $A_{13} = 2$, $A_{22} = (2-v)\psi^2$, $A_{24} = 6$, $A_{12} = A_{14} = A_{21} = A_{23} = 0$ and other A_{ij} ($i = 3, 4$, $j = 1 \sim 4$) are related to k and can be obtained by substituting Eqs. (26) and (27) into Eq. (30). The buckling condition is satisfied when the determinant of the matrix of the coefficients vanishes, with which the k value can be directly calculated.

$$\begin{vmatrix} A_{11} & A_{12} & A_{13} & A_{14} \\ A_{21} & A_{22} & A_{23} & A_{24} \\ A_{31} & A_{32} & A_{33} & A_{34} \\ A_{41} & A_{42} & A_{43} & A_{44} \end{vmatrix} = 0 \tag{32}$$

The exact deflection of the stiffener Eqs. (17) and ((21)) can be captured with infinite series ($n \to \infty$), with which an exact solution of k will be obtained. However, it is unrealistic to use infinite series for the solution. A convergence analysis has been performed, which shows that the obtained k values could maintain five significant figures with $n = 32$. This accuracy is high enough for the current study and all the following results were approximately calculated with $n = 32$. A set of solutions can be calculated for each number of half-waves m, and k is obtained as the minimum positive value of all eigenvalues. Then the lowest value of k is the critical buckling coefficient k_{cr} of the stiffened panel and the corresponding m value indicates its buckling mode in the free upper edge.

After obtaining k_{cr}, the critical buckling strength of the stiffened panel under bending can be calculated by [37]:

$$\sigma_{cr} = \frac{k_{cr}\pi^2 E}{12(1-v^2)} \left(\frac{t_{st}}{h}\right)^2 \tag{33}$$

3.2. Buckling analysis with flexible skin case

This section proposed a new method to first-time consider the effect of flexible skins with non-rigid rotation behaviour on buckling analysis of stiffened panels by combining analytical methods with some basic FE simulations.

The rotation of skin is caused by the non-uniform torsional moment (M_c') along the connecting edge due to the buckling of the stiffener. The torsional moment is equal to the bending moment on the connecting edge of the stiffener (M_c), which is a sinusoid function according to Eqs. (13) and (17). As indicated in Section 3.1, M_c' cannot be obtained analytically for the flexible skin case, FE simulations have been used in this study to investigate the detailed non-rigid rotation behaviour of the flexible skin subjected to a torsional moment with a sinusoid function along the connecting edge. A quarter of the unit skin model with one half-wave region is selected for FE simulations and the corresponding boundary conditions of the model are shown in Fig. 6. The length

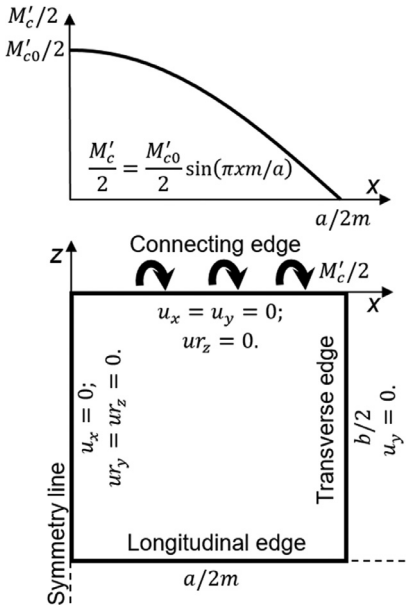

Fig. 6. FE model for the skin subjected to the torsion along the centreline.

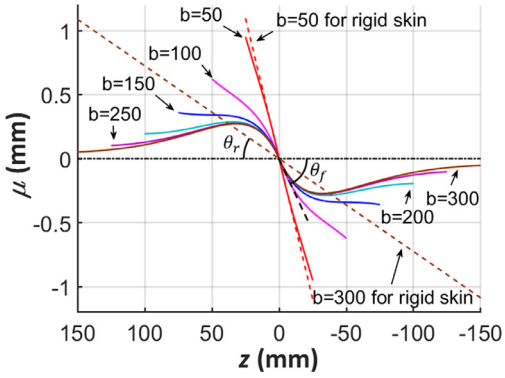

Fig. 7. Deflection of skin in the y-direction (μ) for different skin widths subjected to the same torsion (solid lines are FE simulation results with flexible skins and dashed lines are analytical results with rigid skins).

and width of the model are respectively $a/2m$ and $b/2$, and a torsional moment $M_c'/2$ is considered in the analysis:

$$\frac{M_c'}{2} = \frac{M_{c0}'}{2} \sin\left(\frac{\pi xm}{a}\right) \tag{34}$$

where M_{c0}' is the torsion moment at the joint between the connecting edge and the symmetry line in the whole skin. FE simulations for the models with various width conditions were performed. The geometric sizes of the models include: a length of 50 mm, a thickness of 1 mm and a varying width ranging from 25 mm to 150 mm. As the deformation of the skin subjected to a torsion moment is proportional to the magnitude of the torsion in the elastic region, the value of the torsion moment will not affect the trend of the skin deformation. Hence, M_{c0}' is set as 20 (N m)/m in these FE models for demonstration in this study.

The deflections of the skin at the symmetric line with different skin width conditions from the FE simulation results are shown in Fig. 7 and two analytical results with the rigid skin assumptions are also plotted for comparison. It can be seen that when the width is small, the rotation behaviour of the skin agrees well with the analytical result following the rigid skin assumption, indicating that the rigid skin assumption is satisfied for the skin with a small width. While with the increasing skin width, the cross-section of the skin becomes deformable and distorts heavily, which shows apparent differences with the analytical results,

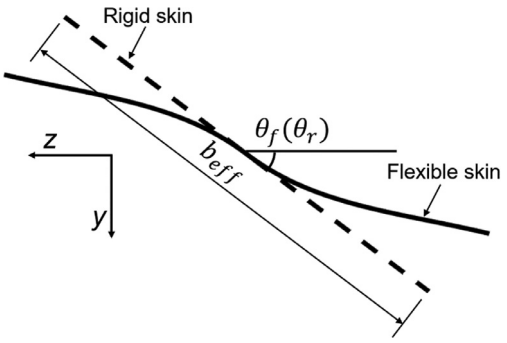

Fig. 8. Schematic diagram of effective width for flexible skin cases.

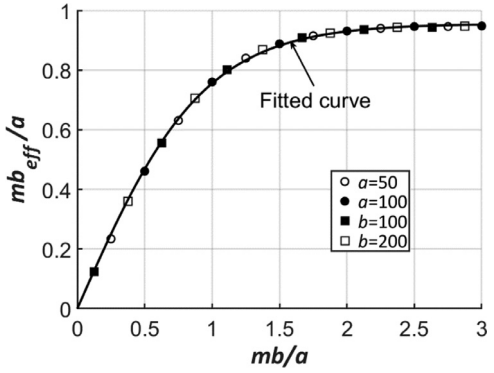

Fig. 9. Evolution of effective width to length ratio mb_{eff}/a versus mb/a of stiffened panels.

and the rigid skin assumption is not appropriate for these cases. In addition, with the increasing skin width, the deformed skins tend to converge to the same shape. This phenomenon can be explained as that the torsion is only applied on the connecting edge of the skin, and its influence region on the flexible skin is thus limited.

M_c' on the connecting edge of skin is only determined by the rotation angle of skin θ' and the torsional stiffness, as indicated in Eq. (6). As shown in Fig. 7, when the skin width is large, the rotation angle between the stiffener and skin in the flexible case θ_f is larger than that in the corresponding rigid skin case θ_r. The larger θ_f in the flexible skin case indicates a smaller torsional stiffness than that with the rigid skin assumption and hence, the analytical solution for rigid skin cases overpredicts the torsional stiffness of skins, leading to inevitable errors of the analytical solution.

Table 1
Geometry of the FE models (unit: mm).

Set 1		Set 2		Set 3		Set 4	
a	*b*	*a*	*b*	*a*	*b*	*a*	*b*
50.0	12.5	100	50.0	800	100	532	200
50.0	37.5	100	100	160	100	229	200
50.0	62.5	100	150	90.0	100	146	200
50.0	87.5	100	200	60.0	100	107	200
50.0	112.5	100	250	47.0	100	84.2	200
50.0	137.5	100	300	38.0	100	69.6	200

In order to overcome this problem, this paper introduces a new concept of effective width, b_{eff}, in the buckling analysis to amend the torsional stiffness according to flexible skin conditions. b_{eff} is defined as the width of an equivalent rigid skin which performs the same torsional stiffness with the flexible skin case having an actual width of b, in which the rotation angle of both skins are the same when they are subjected to the same torsion, as shown in Fig. 8. b_{eff} can be expressed according to the torsional stiffness of the flexible skin GJ_{sk}', as:

$$b_{eff} = \frac{3GJ_{sk}'}{Gt_{sk}^3} = \frac{J_{sk}'b}{J_{sk}} \tag{35}$$

The torsional stiffness of the flexible skin is calculated by torsion divided by the rotation angle per unit length according to Eq. (6), as:

$$GJ_{sk}' = \frac{M_c'}{\frac{\partial^2\theta_f}{\partial x^2}} \tag{36}$$

To obtain the torsional stiffness of the flexible skin from FE simulation results, Eq. (36) is re-written based on the second-order forward difference as:

$$GJ_{sk}' \approx \frac{M_{c0}'\Delta x^2}{(\theta_f)_{x=0} - 2(\theta_f)_{x=\Delta x} + (\theta_f)_{x=2\Delta x}} \tag{37}$$

where Δx is the spatial increment of neighbouring nodes. When Δx tends to 0, b_{eff} achieves an exact value. According to the convergence test on Δx with the criterion of 1% error, Δx is set to $a/20m$.

Substituted Eq. (37) into Eq. (35), the effective width b_{eff} can be calculated, when the rotation angles $(\theta_f)_{x=0}$, $(\theta_f)_{x=\Delta x}$ and $(\theta_f)_{x=2\Delta x}$ are obtained from the FE simulations:

$$b_{eff} \approx \frac{M_{c0}'\Delta x^2}{(\theta_f)_{x=0} - 2(\theta_f)_{x=\Delta x} + (\theta_f)_{x=2\Delta x}} \frac{b}{GJ_{sk}} \tag{38}$$

To investigate the effective width b_{eff} with different skin aspect ratios mb/a, four sets of FE simulations of skins with different dimensions were carried out, as listed in Table 1. The length of the skin is constant with varying skin widths in Sets 1 and 2, while in Sets 3 and 4 the skin width is constant with different skin lengths.

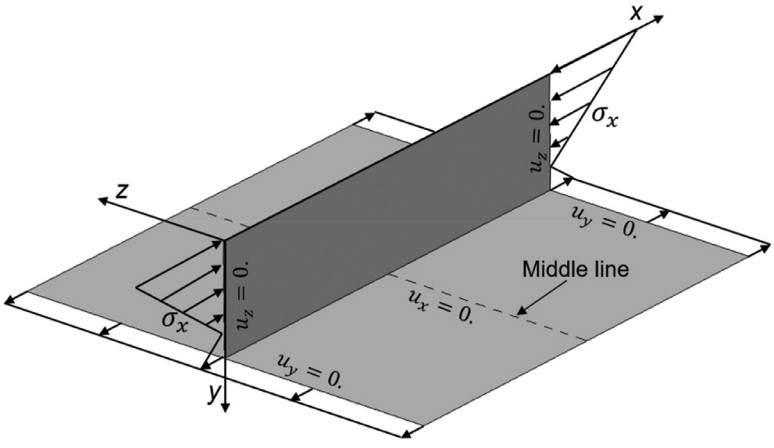

Fig. 10. FE model of a single blade stiffened panel subjected to bending.

Table 2
Geometry and FE results of critical buckling moment and coefficient for test cases.

a (mm)	b (mm)	h (mm)	t_{sk} (mm)	t_{st} (mm)	t_{sk}/t_{st}	α	k	M_{cr} (Nm)
Group 1 (25 mm ≤ a ≤ 200 mm)								
25.0	50.0	25.0	1.00	1.00	1.00	1.18	2.01	42.7
37.5	50.0	25.0	1.00	1.00	1.00	1.18	1.43	30.4
50.0	50.0	25.0	1.00	1.00	1.00	1.18	1.32	28.0
75.0	50.0	25.0	1.00	1.00	1.00	1.18	1.42	30.2
100	50.0	25.0	1.00	1.00	1.00	1.18	1.35	28.6
125	50.0	25.0	1.00	1.00	1.00	1.18	1.37	29.0
150	50.0	25.0	1.00	1.00	1.00	1.18	1.35	28.6
175	50.0	25.0	1.00	1.00	1.00	1.18	1.35	28.6
200	50.0	25.0	1.00	1.00	1.00	1.18	1.35	28.6
Group 2 (12.5 mm ≤ h ≤ 100 mm)								
100	50.0	12.5	1.00	1.00	1.00	1.07	1.33	31.0
100	50.0	14.3	1.00	1.00	1.00	1.09	1.35	30.8
100	50.0	16.7	1.00	1.00	1.00	1.11	1.34	29.9
100	50.0	20.0	1.00	1.00	1.00	1.14	1.30	28.4
100	50.0	25.0	1.00	1.00	1.00	1.18	1.28	27.3
100	50.0	33.3	1.00	1.00	1.00	1.24	1.26	25.7
100	50.0	50.0	1.00	1.00	1.00	1.32	1.24	24.0
100	50.0	66.6	1.00	1.00	1.00	1.39	1.49	27.4
100	50.0	100	1.00	1.00	1.00	1.50	2.23	38.3
Group 3 (50 mm ≤ b ≤ 200 mm)								
100	25.0	25.0	1.00	1.00	1.00	1.32	1.20	23.6
100	50.0	25.0	1.00	1.00	1.00	1.18	1.34	28.6
100	75.0	25.0	1.00	1.00	1.00	1.12	1.34	29.4
100	100	25.0	1.00	1.00	1.00	1.09	1.33	29.7
100	125	25.0	1.00	1.00	1.00	1.07	1.32	29.8
100	150	25.0	1.00	1.00	1.00	1.06	1.31	29.9
100	175	25.0	1.00	1.00	1.00	1.05	1.31	29.8
100	200	25.0	1.00	1.00	1.00	1.04	1.30	30.0
Group 4 (0.25 ≤ t_{sk}/t_{st} ≤ 1)								
50.0	50.0	25.0	0.25	1.00	0.25	1.50	1.02	17.5
50.0	50.0	25.0	0.50	1.00	0.50	1.32	1.07	20.5
50.0	50.0	25.0	0.75	1.00	0.75	1.24	1.19	24.2
50.0	50.0	25.0	1.00	1.00	1.00	1.18	1.32	28.0

The results of the effective width are obtained from the FE modelling results and Eq. (38), and the variation of the effective width to length ratio mb_{eff}/a versus mb/a is shown in Fig. 9. As the results from four sets of models with different geometric parameters of stiffened panels all show the same trend, as shown in Fig. 9, the relationship between mb_{eff}/a and mb/a seems to be independent on the geometric properties of the skin models. mb_{eff}/a increases with a nearly proportional trend with mb/a initially, the increasing speed decreases afterwards with further increasing mb/a values until reaching a saturated level. It is found that this relationship can be perfectly fitted by a hyperbolic tangent equation. For the data shown in Fig. 9, the fitted equation is:

$$b_{eff} = 0.9557 \tanh\left(\frac{1.072mb}{a}\right)\frac{a}{m} \tag{39}$$

By replacing the width b in Eq. (30) with b_{eff}, the non-rigid rotation effect of the flexible skin can be considered for the analytical solution of the buckling analysis. The results and accuracy of the original and updated analytical solutions for stiffened panels with various geometric conditions will be demonstrated and discussed in the following sections.

4. Finite element method

To verify the effectiveness of the analytical solution and the new effective width concept for buckling of stiffened panels introduced in this study, FE simulations were carried out with the commercial software ABAQUS to obtain the critical buckling strength σ_{cr} and the buckling mode of stiffened panels. The buckling coefficient k can be calculated from the obtained σ_{cr} by Eq. (33). The FE model for the stiffened panel is shown in Fig. 10. The model was constrained to a simply supported condition: the two transverse edges of the skin were fixed in the y-direction and the two longitudinal edges were free; the middle line of the skin was fixed in the x-direction and the two transverse edges of stiffener were fixed in the z-direction. The linearly varying stress σ_x representing the bending moment (Eq. (1)) was applied on the two transverse edges of the stiffened panel model. The material was defined as an aluminium alloy with $E = 73.8$ GPa and $\upsilon = 0.33$ [38]. It is documented that the S4R element in ABAQUS can provide accurate solutions for large-scale buckling analysis efficiently [39], and the feasibility and accuracy of the element in solving buckling problems of stiffened panels have been validated in many previous studies [33,40]. Hence, the stiffened panel was modelled with S4R elements in this study. The mesh size convergence analysis was performed and a proper number of elements of the model is selected as 1800, with a mesh of 24 × 50 elements in the skin, and 12 × 50 elements in the stiffener. In ABAQUS, the buckling behaviour is analysed by solving the following equilibrium equations [41]:

$$\left[[k] - \lambda[k]_G\right]\{\delta\} = \{0\} \tag{40}$$

where λ is the buckling load eigenvalue, $[k]$ and $[k]_G$ are stiffness matrices and geometric stiffness matrices and $\{\delta\}$ is the eigenvector.

5. Results and discussion

FE simulations of four groups of stiffened panels with arbitrarily selected different geometric conditions were carried out for comparison and verification. The buckling coefficients k of stiffened panels subjected to bending with different geometric parameters were calculated using the proposed analytical solutions. The critical buckling moment M_{cr}, which is the maximum moment that the stiffened panel can bear without buckling, has also been calculated. Table 2 lists the FE results for the critical buckling moment and coefficient for all the test cases. The effects

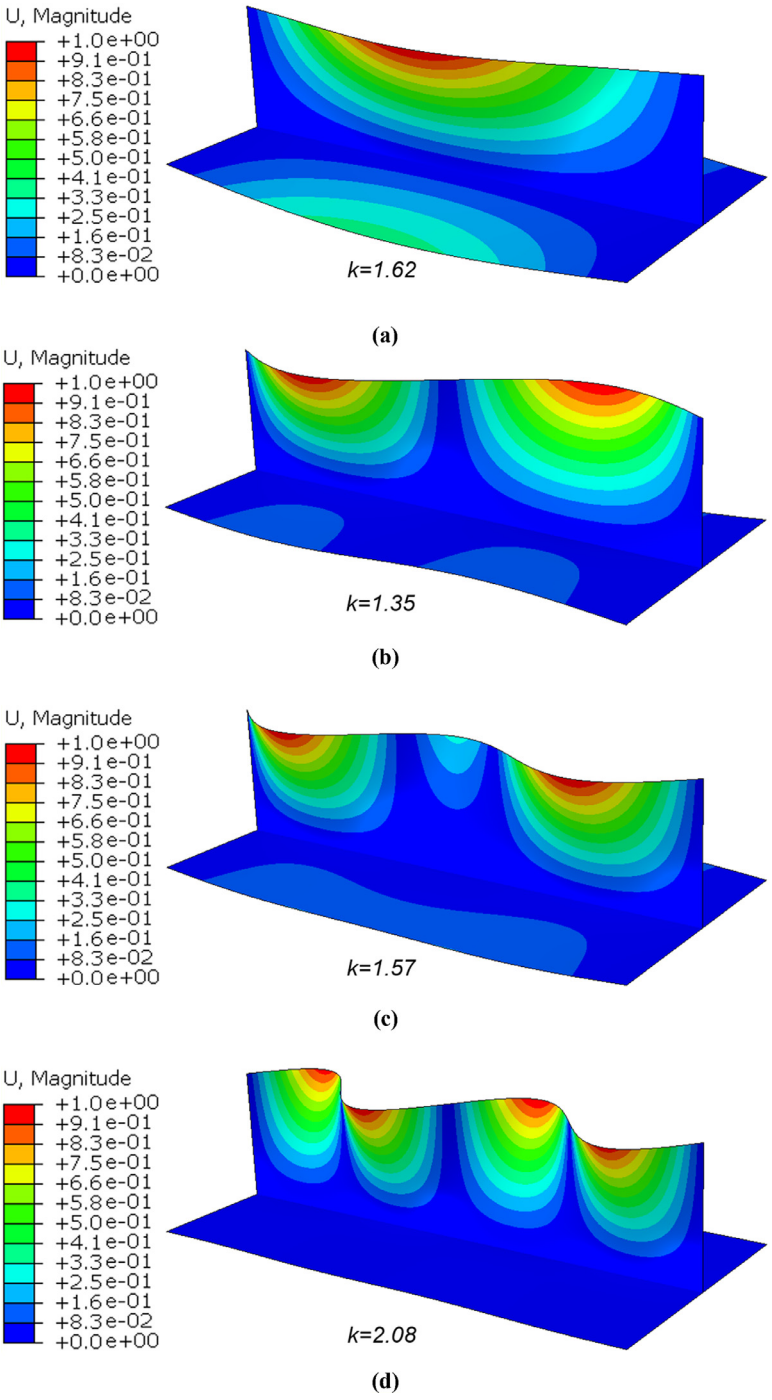

Fig. 11. Buckling mode shapes of a selected stiffened panel ($a = 100$ mm, $b = 50$ mm, $h = 50$ mm, $t_{sk} = 1$ mm, $t_{st} = 1$ mm) for (a) $m = 1$, (b) $m = 2$, (c) $m = 3$ and (d) $m = 4$.

of the four main geometric parameters (stiffened panel length a, stiffened panel width b, stiffener height h and thickness ratio t_{sk}/t_{st}) on the buckling strength of stiffened panels are reported and discussed in the following sections. Although these parameters are arbitrarily selected, they serve to verify the effectiveness of the proposed analytical method. The method can be applied for solving buckling problems of stiffened panels with different geometric parameters.

To visually show the buckling mode shapes of stiffened panels investigated in this study, the FE results of some buckling mode shapes ($m = 1 \sim 4$) of a selected stiffened panel ($a = 100$ mm, $b = 50$ mm, $h = 50$ mm, $t_{sk} = 1$ mm, $t_{st} = 1$ mm) are displayed in Fig. 11. The buckling mode shape in Fig. 11(b) ($m = 2$) is the critical buckling mode since the corresponding buckling coefficient k is the minimum for the selected stiffened panel.

5.1. Effect of stiffened panel length

Buckling analysis of the stiffened panels with various lengths a listed in Table 2 (Group 1) has been performed numerically and analytically with rigid skin and flexible skin assumptions. The obtained k values with different lengths a are shown in Fig. 12. A fair agreement with a slight difference between analytical results with the rigid skin assumption (b) and FE results can be observed in Fig. 12(a). The use of effective stiffened panel width in analytical solution with the flexible skin assumption (b_{eff}) predicts a slight lower k value compared with the rigid skin cases in Fig. 12(a) and achieves an excellent agreement with FE results, as shown in Fig. 12(b). Meanwhile, the critical lengths, at which abrupt changes of the buckling mode exist, become slightly larger with the flexible skin assumption than that with the rigid assumption. The buckling

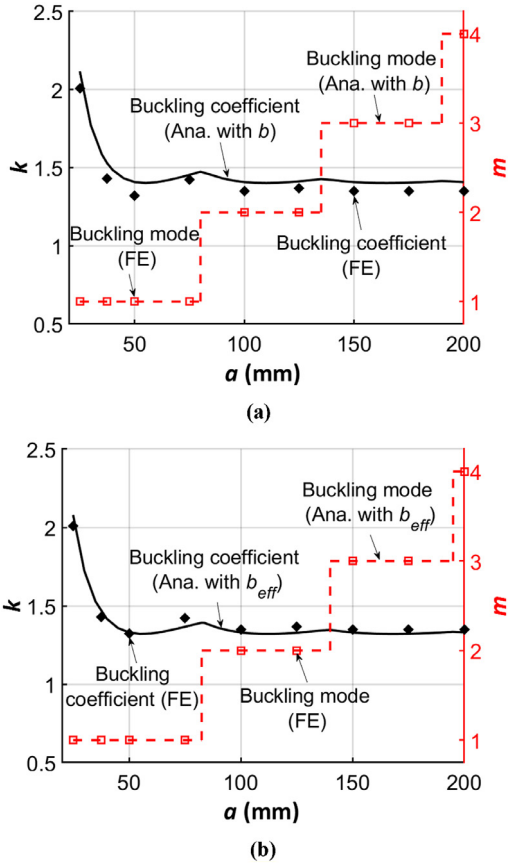

Fig. 12. Buckling coefficient k and buckling mode (half-waves m) versus stiffened panel length a with (a) stiffened panel width in rigid skin assumption and (b) effective stiffened panel width in flexible skin assumption (symbols – FE, lines – analytical results (Ana.)).

Table 3
Original width b and effective width b_{eff} of stiffened panels with different numbers of half-waves m in buckling mode.

	$m=1$	$m=2$	$m=3$	$m=4$
b (mm)	50.0	50.0	50.0	50.0
b_{eff} (mm)	45.9	37.4	28.6	22.9

coefficient k is relatively large with small a values and decreases significantly as a increases. After the buckling coefficient k reaches the minimum value, it begins to increase slightly. The stiffened panel is buckled with a one half-wave pattern ($m=1$) at this stage. The buckling mode of the stiffened panels increases from one half-wave to more half-waves as a increases. Although there is a reducing-increasing cycle for each buckling mode afterwards, it can be seen that the buckling coefficient k remains relatively stable when $m > 1$.

5.2. Effect of stiffener height

According to the equilibrium equation (Eq. (16)), the reciprocal of the stiffener height h^{-1} is relevant to k and their relationship from the tested cases in Table 2 (Group 2) is shown in Fig. 13. The corresponding effective stiffened panel width b_{eff} with different numbers of half-waves m for stiffened panels in Group 2 is calculated according to Eq. (39) and the results are shown in Table 3.

Fig. 13 shows the effect of stiffener height on the buckling coefficient, with b in rigid skin assumption in Fig. 13(a) and b_{eff} in flexible skin assumption in Fig. 13(b) respectively. The differences of buckling coefficient between the analytical results with the actual width and corresponding FE results increases when the reciprocal of the stiffener height increases, due to the increasing difference between b_{eff} and b with increasing m, as listed in Table 3. An apparent improvement in buckling coefficient prediction has been achieved when b_{eff} in flexible skin assumption was used, which shows an excellent agreement with corresponding FE results.

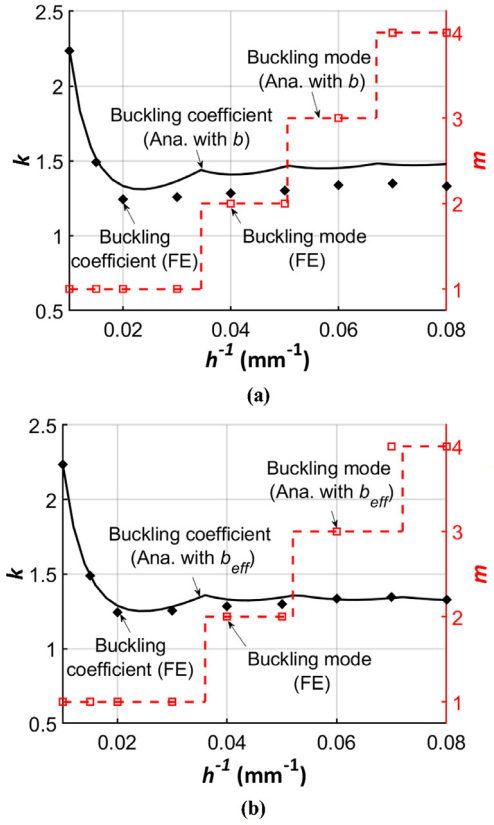

Fig. 13. Buckling coefficient k and buckling mode (half-waves m) versus reciprocal of stiffener height h^{-1} with (a) stiffened panel width b in rigid skin assumption and (b) effective stiffened panel width b_{eff} in flexible skin assumption (symbols – FE, lines – analytical results (Ana.)).

The effect of h^{-1} on the buckling coefficient k is similar to that of the stiffened panel length a. The buckling coefficient decreases abruptly first and then increases slightly as h^{-1} increases when the buckling mode is of one half-wave ($m=1$) pattern, and a repeated slight reducing-increasing cycle of buckling coefficient exists for subsequent buckling modes. In the later stage, the buckling coefficient increases as the skin rotation constraints coefficient C_r increases. According to Eq. (29), C_r is positively related to the variables of m^2, b_{eff} and h. When h^{-1} increases, though b_{eff} and h decrease, C_r still increases first at each buckling mode due to the increase of m.

5.3. Effect of stiffened panel width

In this section, the effect of stiffened panel width on buckling behaviour of stiffened panels is discussed according to the test cases in Table 2 (Group 3). The analytical results of the buckling coefficient k calculated with b in rigid skin assumption and b_{eff} in flexible skin assumption versus the stiffened panel width b are respectively compared with corresponding FE results in Fig. 14(a) and (b). A larger difference between the analytical results with b in rigid skin assumption and FE results can be observed when the stiffened panel width increases, while the accuracy of analytical results is significantly improved with b_{eff} in flexible skin assumption. The high accuracy of analytical solution with

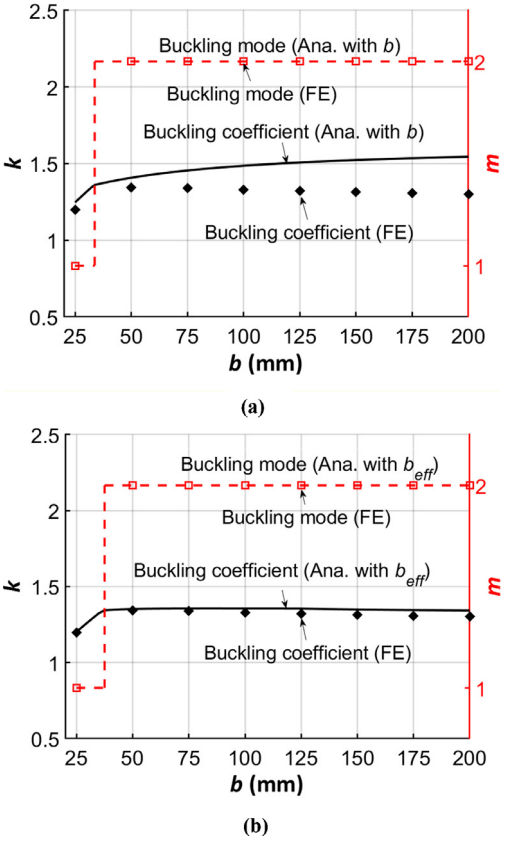

Fig. 14. Buckling coefficient k and buckling mode (half-waves m) versus panel width b with (a) stiffened panel width b in rigid skin assumption and (b) effective stiffened panel width b_{eff} in flexible skin assumption (symbols – FE, lines – analytical results (Ana.)).

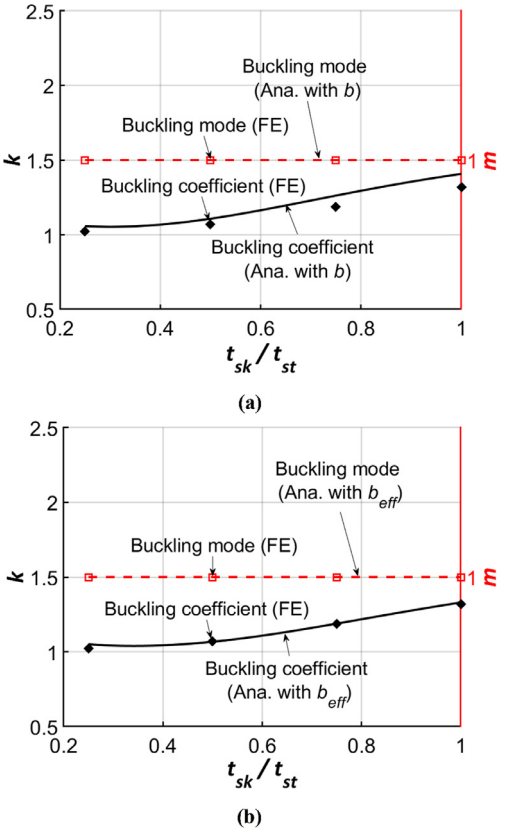

Fig. 15. Buckling coefficient k and buckling mode (half-waves m) versus thickness ratio t_{sk}/t_{st} with (a) stiffened panel width b in rigid skin assumption and (b) effective stiffened panel width b_{eff} in flexible skin assumption (symbols – FE, lines – analytical results (Ana.)).

b_{eff} is verified by the numerical results. The buckling coefficient k increases with a small stiffened panel width, and then becomes stable with a slightly dropping trend as the stiffened panel width increases. The buckling mode of the stiffened panel changes from one half-wave mode ($m=1$) to two half-waves mode ($m=2$), when k reaches the stable level.

According to Eqs. (19), (30) and (39), there are three factors related to the stiffened panel width that affect k, namely, skin rotational constraint (C_r), flexible skin effect (b_{eff}) and loading coefficient (α). C_r increases when the stiffened panel width increases, leading to the initial increase of k in Fig. 14. Since the flexible skins tend to deform to the same shape with increasing stiffened panel width, as shown in Fig. 7, the effective width b_{eff} remains relatively stable with high stiffened panel width conditions, and thus, a comparatively stable value of k can be observed in Fig. 14. In addition, the loading coefficient α declines when the stiffened panel width b increases, which contributes to the slight decrease of the buckling coefficient k with further increasing stiffened panel width.

5.4. Effect of thickness ratio

The effect of the thickness ratio t_{sk}/t_{st} on the buckling coefficient k is discussed with geometric parameters given in Table 2 (Group 4). The results of k calculated by b and b_{eff} versus t_{sk}/t_{st} are shown in Fig. 15(a) and (b). The analytical results with b show a good agreement with FE results at low t_{sk}/t_{st} values, however, the difference between them increases with increasing t_{sk}/t_{st} values. Meanwhile, results with b_{eff} show an excellent agreement at all t_{sk}/t_{st} values investigated in this study, demonstrating the prediction accuracy of the proposed analytical solution using b_{eff}. Increasing thickness ratio leads to the increase of the skin rotational constraint according to Eq. (30), and thus, resulting in a larger buckling coefficient, as shown in Fig. 15.

According to the parametric study in this section, the effects of a and h^{-1} on the buckling coefficient of stiffened panels are similar. Especially, the effects are significant when a/h is small. b has a small effect on the buckling coefficient when it is relatively large due to the twist of flexible skin, while the increase of t_{sk}/t_{st} will increase buckling coefficient. As demonstrated in the comparison with FE simulations, the proposed analytical solution with the new parameter, effective width, achieves a very high accuracy to calculate the buckling strength of the stiffened panels under bending.

Although the analytical method for buckling analysis is developed based on stiffened panels with one blade stiffener in this study, it can be extended for stiffened panels with other types of single stiffener (such as T-, Z-, J- shapes) or multiple stiffeners, by modifying the boundary conditions of the simplified model according to particular cases. For example, the buckling problem of stiffened panels with a T-shape stiffener can be directly calculated by replacing the free boundary condition for the top of the simplified model in this study to an elastically built-in boundary condition. To consider the buckling analysis of stiffened panels with multiple stiffeners, the boundary condition at the longitudinal edge of the stiffened panels can be modified from free to symmetric boundary condition (rotation angle equal zero) or antisymmetric boundary condition (transverse displacement equal zero), and the effective width with the new boundary conditions, which is obtained by the FE assisted method, can be employed in the analytical solution. The analytical method proposed in this study can be used to guide the design of stiffened panels and applied to investigate the limit curvature radius and/or the optimal geometric parameters of stiffened panels subjected to a bending moment during forming processes to avoid possible buckling.

6. Conclusions

An analytical solution for the elastic buckling analysis of stiffened panels subjected to pure bending has been developed in this study, whose effectiveness has been verified by corresponding FE simulations of some selected cases. Based on the developed analytical solution, the effect of the main geometric parameters of stiffened panels on their buckling strengths has been discussed. The following conclusions can be drawn:

1 The buckling problem of a stiffened panel subjected to bending can be simplified as a stiffener with a special elastically built-in boundary condition to consider the effect of skin-stiffener interaction. The analytical solution proposed for this simplified model can effectively calculate the critical buckling strength of stiffened panels.
2 A new concept of effective width (b_{eff}) is proposed for buckling analysis of stiffened panels to account for the flexible skin conditions in real cases, and a particular relationship between mb_{eff}/a and mb/a, which is independent on the geometric properties of stiffened panels, has been quantitatively obtained through an FE assisted method. It significantly improves the accuracy for buckling strength prediction and reduces the maximum difference between analytical results and simulation results from 12.2% with the conventional rigid skin assumption to only 3.9%.
3 The buckling coefficient k of stiffened panels decreases abruptly with increasing length a at first, and stays at a relatively stable level with further increase of the length when the buckling mode of stiffened panels changes from one half-wave ($m=1$) to higher order half-waves. The reciprocal of the stiffener height h^{-1} shows a similar effect on k.
4 With increasing stiffened panel width b, the buckling coefficient initially increases and then becomes stable with an insignificant decrease. Meanwhile, the increasing thickness ratio t_{sk}/t_{st} leads to the increase of the skin rotational constraint, resulting in a larger buckling coefficient.

Acknowledgements

The strong support from the Aviation Industry Corporation of China (AVIC) Manufacturing Technology Institute (MTI) (grant no. MESM_P42748) for this funded research is much appreciated. The research was performed at the AVIC Centre for Structural Design and Manufacture at Imperial College London.

References

[1] Munroe J, Wilkins K, Gruber M, Domack MS. Integral Airframe Structures (IAS): validated feasibility study of integrally stiffened metallic fuselage panels for reducing manufacturing costs; 2000. Tech Rep NASA/CR-2000-209337.
[2] Pettit RG, Wang JJ, Toh C. Validated feasibility study of integrally stiffened metallic fuselage panels for reducing manufacturing costs – The Boeing Company; 2000. Tech Rep NASA/CR-2000-209342.
[3] Zhao Y, Zhou L, Wang Q, Yan K, Zou J. Defects and tensile properties of 6013 aluminum alloy T-joints by friction stir welding. Mater Des 2014;57:146–55. doi:10.1016/J.MATDES.2013.12.021.
[4] Lynch C, Murphy A, Price M, Gibson A. The computational post buckling analysis of fuselage stiffened panels loaded in compression. Thin-Walled Struct 2004;42:1445–64. doi:10.1016/j.tws.2004.04.002.
[5] Lam ACL, Shi Z, Yang H, Wan L, Davies CM, Lin J, et al. Creep-age forming AA2219 plates with different stiffener designs and pre-form age conditions: experimental and finite element studies. J Mater Process Technol 2015;219:155–63. doi:10.1016/j.jmatprotec.2014.12.012.
[6] Yan Y, Wan M, Wang H. FEM equivalent model for press bend forming of aircraft integral panel. Trans Nonferrous Met Soc China 2009;19:414–21. doi:10.1016/S1003-6326(08)60288-5.
[7] Yan Y, Wang H, Wan M. Prediction of fracture in press bend forming of aluminum alloy high-stiffener integral panels. Comput Mater Sci 2011;50:2232–44. doi:10.1016/J.COMMATSCI.2011.02.034.
[8] Zhan L, Lin J, Dean TA. A review of the development of creep age forming: experimentation, modelling and applications. Int J Mach Tools Manuf 2011;51:1–17. doi:10.1016/j.ijmachtools.2010.08.007.
[9] Hua L, Han X. Theory and application of space envelope forming (SEF), jinan, China. 13th international conference on frontiers of design and manufacturing (ICFDM2018); 2018.
[10] Han X, Hua L, Zhuang W, Zhang X. Process design and control in cold rotary forging of non-rotary gear parts. J Mater Process Technol 2014;214:2402–16. doi:10.1016/J.JMATPROTEC.2014.05.003.
[11] Han X, Zhang X, Hua L. Calculation method for rocking die motion track in cold orbital forging. J Manuf Sci Eng 2015;138:014501. doi:10.1115/1.4030855.
[12] Han X, Hu Y, Hua L. Cold orbital forging of gear rack. Int J Mech Sci 2016;117:227–42. doi:10.1016/J.IJMECSCI.2016.09.007.
[13] Lyu F, Li Y, Huang X, Shi Z, Zeng Y, Lin J. An investigation of creep age forming of AA7B04 stiffened plates: experiment and FE modelling. J Manuf Process 2019;37:232–41. doi:10.1016/J.JMAPRO.2018.11.031.
[14] Zhang S, Khan I. Buckling and ultimate capability of plates and stiffened panels in axial compression. Mar Struct 2009;22:791–808. doi:10.1016/J.MARSTRUC.2009.09.001.
[15] Nguyen-Thoi T, Bui-Xuan T, Phung-Van P, Nguyen-Xuan H, Ngo-Thanh P. Static, free vibration and buckling analyses of stiffened plates by CS-FEM-DSG3 using triangular elements. Comput Struct 2013;125:100–13. doi:10.1016/J.COMPSTRUC.2013.04.027.
[16] Bisagni C, Vescovini R. Analytical formulation for local buckling and post-buckling analysis of stiffened laminated panels. Thin-Walled Struct 2009;47:318–34. doi:10.1016/J.TWS.2008.07.006.
[17] Rahbar-Ranji A. Elastic buckling analysis of longitudinally stiffened plates with flat-bar stiffeners. Ocean Eng 2013;58:48–59. doi:10.1016/j.oceaneng.2012.09.018.
[18] Durban D, Zuckerman Z. Elastoplastic buckling of rectangular plates in biaxial compression/tension. Int J Mech Sci 1999;41:751–65. doi:10.1016/S0020-7403(98)00055-1.
[19] Li R, Zheng X, Wang H, Xiong S, Yan K, Li P. New analytic buckling solutions of rectangular thin plates with all edges free. Int J Mech Sci 2018;144:67–73. doi:10.1016/J.IJMECSCI.2018.05.041.
[20] Timoshenko S.P., Gere J.M. Theory of elastic stability 1961.
[21] Thompson JMT, Hunt GW. A general theory of elastic stability. London: J. Wiley; 1973.
[22] Leissa AW, Kang J-H. Exact solutions for vibration and buckling of an SS-C-SS-C rectangular plate loaded by linearly varying in-plane stresses. Int J Mech Sci 2002;44:1925–45. doi:10.1016/S0020-7403(02)00069-3.
[23] Kang J-H, Leissa AW. Exact solutions for the buckling of rectangular plates having linearly varying in-plane loading on two opposite simply supported edges. Int J Solids Struct 2005;42:4220–38. doi:10.1016/j.ijsolstr.2004.12.011.
[24] Stowell EZ, Lundquist EE. Critical compressive stress for flat rectangular plates supported along all edges and elastically restrained against rotation along the unloaded edges; 1942. NACA Tech Rep-733.
[25] Johnson JH Jr, Noel RG. Critical bending stress for flat rectangular plates supported along all edges and elastically restrained against rotation along the unloaded compression edge. J Aeronaut Sci 1953;20:535–40. doi:10.2514/8.2722.
[26] Madhavan M, Davidson JS. Buckling of centerline-stiffened plates subjected to uniaxial eccentric compression. Thin-Walled Struct 2005;43:1264–76. doi:10.1016/J.TWS.2005.03.013.
[27] Paik JK, Thayamballi AK. Buckling strength of steel plating with elastically restrained edges. Thin-Walled Struct 2000;37:27–55. doi:10.1016/S0263-8231(00)00009-4.
[28] Bulson PS. The stability of flat plates. Elsevier Publishing Company; 1969.
[29] Wang CM, Aung TM. Plastic buckling analysis of thick plates using p-Ritz method. Int J Solids Struct 2007;44:6239–55. doi:10.1016/J.IJSOLSTR.2007.02.026.
[30] Chen Y. Ultimate strength analysis of stiffened panels using a beam-column method PhD thesis. Virginia Tech; 2003.
[31] Ma M. Elastic and inelastic analysis of panel collapse by stiffener buckling PhD thesis. Virginia Tech; 1994.
[32] Hughes OF, Ma M. Elastic tripping analysis of asymmetrical stiffeners. Comput Struct 1996;60:369–89. doi:10.1016/0045-7949(95)00389-4.
[33] Fujikubo M, Yao T. Elastic local buckling strength of stiffened plate considering plate / stiffener interaction and welding residual stress. Mar Struct 1999;12:543–64.
[34] Byklum E, Amdahl J. A simplified method for elastic large deflection analysis of plates and stiffened panels due to local buckling. Thin-Walled Struct 2002;40:925–53. doi:10.1016/S0263-8231(02)00042-3.
[35] Chong ACM, Yang F, Lam DCC, Tong P. Torsion and bending of micron-scaled structures. J Mater Res 2001;16:1052–8. doi:10.1557/JMR.2001.0146.
[36] Barsoum RS, Gallagher RH. Finite element analysis of torsional and torsional-flexural stability problems. Int J Numer Methods Eng 1970;2:335–52. doi:10.1002/nme.1620020304.
[37] Niu MC-Y. Airframe stress analysis and sizing. Hong Kong: Conmilit Press; 1997.
[38] Yang H. Creep age forming investigation on aluminium alloy 2219 and related studies PhD thesis. Imperial College London; 2013.
[39] Hibbitt H, Karlsson B, Sorensen P. Abaqus analysis user's manual version 6.10. Providence, RI, USA: Dassault Systèmes Simulia Corp.; 2010.
[40] Vescovini R, Bisagni C. Two-step procedure for fast post-buckling analysis of composite stiffened panels. Comput Struct 2013;128:38–47. doi:10.1016/j.compstruc.2013.06.002.
[41] Mukhopadhyay M, Mukherjee A. Finite element buckling analysis of stiffened plates. Comput Struct 1990;34:795–803. doi:10.1016/0045-7949(90)90350-B.